Hussain, Javed; Jonsson, Hannes; Skulason, Egill

Calculations of Product Selectivity in Electrochemical CO2 Reduction

Published in:
ACS Catalysis

DOI:
10.1021/acscatal.7b03308

Published: 01/06/2018

Document Version
Publisher's PDF, also known as Version of record

ACS Catalysis

Research Article

Cite This: ACS Catal. 2018, 8, 5240−5249

pubs.acs.org/acscatalysis

Calculations of Product Selectivity in Electrochemical CO_2 Reduction

Javed Hussain,[†] Hannes Jónsson,[†,‡] and Egill Skúlason*[,†]

[†]Science Institute and Faculty of Physical Sciences, University of Iceland VR-III, 107 Reykjavík, Iceland

[‡]Department of Applied Physics, Aalto University, Espoo FI-00076, Finland

Supporting Information

ABSTRACT: CO_2 can be reduced electrochemically to form valuable chemicals such as hydrocarbons and alcohols using copper electrodes, whereas the other metal electrodes tested so far mainly form CO or formate, or only the side product, H_2. Accurate modeling of electrochemical reaction rates including the complex environment of an electrical double layer in the presence of an applied electrical potential is challenging. We show here that calculated rates, obtained using a combination of density functional and rate theory, are in close agreement with available experimental data on the formation of the various products on several metal electrodes and over a range in applied potential, thus demonstrating the applicability of the theoretical methodology. The results explain why copper electrodes give a significant yield of hydrocarbons and alcohols, and why methane, ethylene, and ethanol are formed in electroreduction rather than methanol, which is the main product when H_2 gas reacts with CO_2 on copper catalyst. The insight obtained from the calculations is used to develop criteria for identifying new and improved catalysts for electrochemical CO_2 reduction.

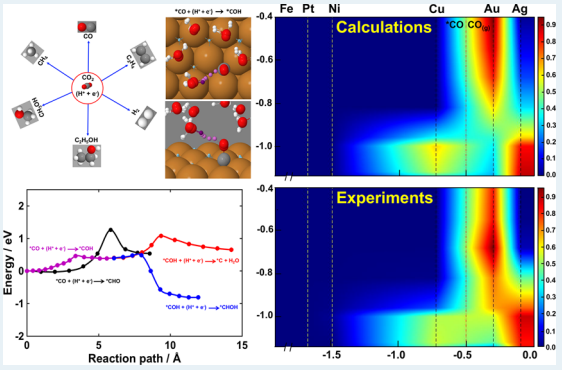

KEYWORDS: *reaction mechanism, electrochemical CO_2 reduction reaction, electrocatalysis, density functional theory calculations, selectivity*

INTRODUCTION

The development of systems capable of reducing CO_2 can help establish a carbon-neutral economy.[1] A particularly appealing approach is to use CO_2 as a reactant and a renewable energy source such as geothermal, wind, or solar energy to make synthetic fuel in small-scale, decentralized devices.[2] This can be an efficient way to store surplus electrical energy as chemical energy that can be utilized when needed in mobile as well as stationary applications. An understanding of the electrochemical reduction of CO_2 can, furthermore, help in the development of artificial photosynthesis.

The possibility of direct electrochemical CO_2 reduction reaction (CO_2RR) has been demonstrated in laboratory experiments.[3−16] A significant yield (70% current efficiency) of CH_4, C_2H_4, and C_2H_5OH has been obtained by using copper electrodes and an applied potential of ca. −1 V (all values are given with respect to the reversible hydrogen electrode, RHE). Other metal electrodes tested so far do not produce a significant yield of either hydrocarbons or alcohols. Electrodes made of Ti, Fe, Ni, or Pt form hydrogen almost exclusively, while CO is the major product on Ag, Au, and Zn electrodes and formate is mainly formed on Pb, Hg, Tl, In, Sn, Cd, and Bi electrodes.[5] Most of the experiments have been carried out with polycrystalline electrodes, but some experiments have been done using single crystal electrodes with either Cu(111) or Cu(100) surface exposed.[7,16] The primary difference between the reaction at the two facets lies in the C_2H_4 formation which occurs more readily on Cu(100).[7]

While the results obtained for copper electrodes is encouraging, catalysts with smaller overpotential, higher activity, and greater selectivity need to be developed to make electrochemical reduction of CO_2 commercially viable. Theoretical calculations could help identify the reaction mechanism and predict which materials are likely to be a better electrocatalyst than Cu for this important reaction. However, the first task is to test whether the currently available theoretical methodology for describing such systems is accurate enough by comparing calculated results with the various available experimental results.

Calculations using density functional theory (DFT) have become a powerful tool for studying catalytic processes and have helped identify new and improved catalysts.[17−20] The results of such calculations can give mechanistic insight that is hard to obtain from experiments alone. Electrochemical systems are complex, however, and the modeling of electrocatalytic processes is still undergoing rapid development.[21−26] In addition to the usual aspects of catalysis, such as the binding of intermediates to the catalyst surface and activation energy of the elementary steps, it is important to take into account the

Received: September 26, 2017
Revised: April 18, 2018
Published: April 23, 2018

DOI: 10.1021/acscatal.7b03308
ACS Catal. 2018, 8, 5240−5249

interaction with the electrolyte and the presence of an applied potential.

Most computational studies of electrochemistry in recent years have been carried out using a model where the binding free energy of intermediates is evaluated and shifted according to the applied voltage without evaluating reaction paths and activation energy of the elementary steps.[27] We will refer to this as the thermochemical model (TCM). The TCM approach has been successful and has led to suggestions of improved catalysts for the hydrogen evolution reaction (HER)[17] and oxygen reduction reaction (ORR).[18] For these reactions, the mechanism is quite well-known.[28,29] The TCM approach has also been applied in calculations of CO_2RR.[30−38] The reaction mechanism for CH_4 formation predicted by TCM on flat Cu(111)[31] and stepped Cu(211)[30,32] surfaces is

$$CO_2 \rightarrow *COOH \rightarrow *CO \rightarrow *CHO \rightarrow *CH_2O \rightarrow *OCH_3 \rightarrow CH_4$$

The CO_2RR is a more complex system than HER or ORR. At least 15 different carbon-containing final products have been identified experimentally[8] in addition to the side reaction, H_2 formation, and product selectivity and reaction rates have been shown to vary strongly with applied potential.

Several calculations have been carried out where the activation energy of reaction steps is calculated at near zero voltage and the value then shifted by $-peU$, where the parameter p has a value between 0 and 1 (usually around 1/2), to take into account the effect of applied potential.[39−42] These calculations have given a different mechanism of CO_2RR past CO on Cu(111)[39]

$$*CO \rightarrow *COH \rightarrow *C \rightarrow *CH \rightarrow *CH_2 \rightarrow *CH_3 \rightarrow CH_4$$

and on Cu(211)[42]

$$*CO \rightarrow *CHO \rightarrow *CHOH \rightarrow *CH \rightarrow *CH_2 \rightarrow *CH_3 \rightarrow CH_4$$

A more detailed calculation of CH_4 formation, based on the evaluation of the activation energy of each step as a function of applied potential and including the presence of water molecules and hydronium ions, has given a substantially different reaction mechanism on Cu(111) electrodes at around −1 V[43,44]

$$CO_2 \rightarrow *COOH \rightarrow *CO \rightarrow *COH \rightarrow *CHOH \rightarrow *CH_2OH \rightarrow *CH_2 \rightarrow *CH_3 \rightarrow CH_4$$

Other calculations have more recently given the same mechanism.[49]

Calculations have also been carried out to investigate the possibility of C−C bond formation in, for example, CO−CO, CO−CHO, or CO−COH species on Cu(111), Cu(100), and Cu(211) surfaces.[45−51] The calculations have shown that C−C bond formation is indeed more facile on the Cu(100) facet.

The microscopic structure of the solid−liquid interface in the presence of applied potential and an electrolyte is not well known. Recent experimental and theoretical work has addressed how the presence of anions[52,54] and cations[15,52,53,55,56] affects CO_2RR. The distance of these ions from the surface can differ depending on the metal and the applied potential.[15,53,54,56] For Cu(111), it has been concluded that neither I^- nor K^+ are adsorbed on the surface at the applied potential relevant for CO_2RR.[54] Most experiments on CO_2RR have been performed with 0.1 M $KHCO_3$ solution with pH = 6.8. While the pK_a value for hydrolysis of the hydrated potassium ion is 14.5,[57] the effect of electrical field close to the Cu electrode at −1.0 V is predicted to drop to 8.5 and change the pH to 7.5.[15] Hydrolysis could then occur near the electrode to form hydronium ions that can be transferred via Grotthuss mechanism. Overall, these model results indicate that the potassium ions are located in the outer Helmholtz layer,[15,56] and they facilitate the hydrolysis of water providing hydronium ions for the double layer.

We present here results of a comprehensive study involving detailed simulations for a number of metal electrodes (Cu, Pt, Au, Ag, Ni, Fe, Rh, Ir) where the current efficiency of CO_2RR formation of various products has been estimated over a range in applied potential. DFT and rate theory is used to calculate the energetics and estimate the rates of the various electrochemical processes using an atomic scale model of the charged solid−liquid interface where the effect of the applied potential on the activation energy for each proton−electron transfer step is obtained. The results are found to be in excellent agreement with the available experimental data. From these results, the reason for the special catalytic activity of copper electrodes can be identified and a two-parameter criterion formulated for identifying a better catalyst for electrochemical CO_2 reduction to hydrocarbons and alcohols.

METHODS

The methodology used here has previously been applied in theoretical studies of electrochemical reactions: The hydrogen evolution reaction (HER)[28,44,58,59] and the oxygen reduction reaction[29] on Pt(111), as well as CH_4 formation by CO_2RR on Cu(111).[43,44] In order to reduce the size of the simulated system as much as possible, the solvent is included as bilayer of ice with variable concentration of hydronium ions. The electrical double layer is simulated by adding H atoms to create solvated protons and excess electrons in the metal electrode.[26,28,58,59] Every other H_2O molecule at the interface points one of its H atoms toward the electrode while the other H_2O molecules are in the plane of the surface, consistent with reducing conditions.[60] We have chosen to use the same bilayer model for all the metals investigated here since the main focus is to compare the effect of the metals and the applied potential on the catalytic rate and selectivity in CO_2RR, even though classical trajectory simulations have shown that the ice bilayer is not stable at inert surfaces, such as Au(111) and Ag(111), but brakes up on the time scale of a few ps.[61]

By varying the number of H atoms added to the bilayer, the corresponding electrostatic potential difference over the double layer can be tuned (see further Figure S1 in the Supporting Information). The more H atoms are added, the more negative the potential becomes. The work function is evaluated from the long-range, asymptotic value of the effective potential of an electron in the vacuum region for the initial, saddle point, and final states of each of the reaction steps that involve a direct addition of a proton from the water layer and an electron from the electrode. In order to convert the calculated work function to an electrical potential with respect to the standard hydrogen electrode (SHE), the free energy stored in the double layer is calculated for several proton−electron concentrations as a function of the work function of the systems. The relationship is parabolic because the double layer is a capacitor and the

DOI: 10.1021/acscatal.7b03308
ACS Catal. 2018, 8, 5240−5249

minimum of the parabola corresponds to zero voltage vs SHE.[28,59,62] The potential of zero charge calculated in this way for several close-packed transition metal electrodes has been found to be in reasonable agreement with experimental measurements.[62] We convert the applied potential scale from SHE at pH = 0 to the RHE scale at pH = 6.8 with $U_{RHE} = U_{SHE} + k_B T$ pH = U_{SHE} + 0.059 V pH at room temperature. Because of the finite size of the simulated system, a change in the number of protons present results in a change in the corresponding potential. An extrapolation scheme involving calculations of several systems of different size but corresponding to the same electrical potential initially is used to estimate the activation energy of each step at a fixed potential (Figure S2).[28,59] An extrapolation is carried out to an infinite system where the potential does not change as a proton reacts. The coverage of hydrogen adatoms is adjusted according to the applied potential. For 0 to −1 V, the coverage is nearly a full ML on Cu(111), but a full ML coverage and beyond can be reached when the applied potential is more negative than −1 V (see Figure S3). The admolecules formed from CO_2 are added to the surfaces below or in the middle of the honeycomb bilayer except for the species that undergo reduction resulting in a release of a water molecule. There, one of the water molecules is removed to make room for the water molecule that is formed during the reaction. This is done for the following reactions: *COOH + $(H^+ + e^-)$ → *CO + H_2O, *COH + $(H^+ + e^-)$ → *C + H_2O, *CHOH + $(H^+ + e^-)$ → *CH + H_2O, and *CH_2OH + $(H^+ + e^-)$ → *CH_2 + H_2O.

Calculations were carried out for all possible intermediates of CO_2RR on all the metals discussed and the activation energy evaluated for each of the possible elementary reduction steps. The rate of each elementary step was estimated using the harmonic approximation to transition state theory, where the rate constant is expressed as

$$k = \nu_{eff} e^{-E_a/k_B T} \quad (1)$$

The activation energy, E_a, was calculated by determining the MEP using the climbing image nudged elastic band (CI-NEB) method.[63−65] The calculations were considered to be converged when the magnitude of the gradient of the energy at the climbing image had dropped below 0.03 eV/Å. In some of the cases the Hessian was evaluated to verify that it had one and only one negative eigenvalue. The highest energy along an MEP minus the energy of the initial state minimum gives the activation energy.

The rate of an elementary step at a reactive site on the surface is the rate constant times the probability of having the reactants present at the site. The value of the pre-exponential factor, ν, was taken to be 10^{13} $s^{-1}site^{-1}$, and the fact that reactants are not present at all sites was taken into account roughly by using the following values of an effective pre-exponential factor (ν_{eff}) (in units of s^{-1} $site^{-1}$), Cu: CO_2RR = 10^8 and HER = 10^{12}, Pt: CO_2RR = 10^{10} and HER = 10^{10}, Fe: CO_2RR = 10^{10} and HER = 10^{11}, Ni: CO_2RR = 10^9 and HER = 10^9, Au: CO_2RR = 10^{12} and HER = 10^{12}, Ag: CO_2RR = 10^{11} and HER = 10^{13}. For a given metal, the same value of the ν_{eff} was used for the whole range in applied potential and for all CO_2RR products. Note, the ν_{eff} is never higher for CO_2RR than HER because the coverage of carbon-containing species is not expected to be as high as the proton coverage at the double layer. This small variation in the value of the ν_{eff} does, however, not change any of the trends deduced from the calculations and would correspond to a 0.1 eV variation in calculated activation energy, i.e. within the uncertainty of DFT calculations (Figure S4). The surface area (in units of cm^2) per site, A/N, on Cu(111), Au(111), Ag(111), Pt(111), Ni(111), Ir(111), Rh(111) and Fe(110) is 6.13×10^{-16}, 6.97×10^{-16}, 6.95×10^{-16}, 6.64×10^{-16}, 5.88×10^{-16}, 6.39×10^{-16}, 6.36×10^{-16}, and 4.81×10^{-16}, respectively. The current density is evaluated as $i = keN/A$, where e is the electron charge and k is calculated by eq 1.[28] The current efficiency for a given product is the current density corresponding to that product divided by the total current density. In this work, we take the total current density to be the current density of a given product (methane or CO) and the current density of H_2 formation, both for the experimental data and the calculated results.

Experimentally, it has been shown that mass transport effects are negligible for all the reported applied potentials for Cu electrodes, while for Au and Ag mass transport limitations start at −1.0 and −1.3 V, respectively.[14] We did not correct for mass transport effects in the theoretical calculations because they have been estimated to be negligible in the range of the applied potential reported here.

The electronic structure calculations were carried out using density functional theory (DFT) within the RPBE generalized gradient functional approximation[66] using the VASP software.[67] A plane wave basis set with a cutoff energy of 350 eV was used in the representation of the valence electrons and projector augmented wave (PAW) used to represent core electrons.[68] Test calculations using a cutoff energy of 400 eV gave the same results to within 20 meV. The electrodes were first represented by slabs of three layers of metal atoms during searches for minima and saddle points, and the metal atoms in the top layer were allowed to move as well as the adsorbed species and the water layer. Single-point calculations with 9 metal layers were subsequently carried out in order to converge the energetics with respect to the number of layers (Table S1). The electrodes were represented by periodically repeated slabs with (2 × 3), (4 × 3), and (4 × 6) surface cells combined with (6 × 4 × 1), (3 × 4 × 1), and (3 × 2 × 1) k-point sampling, respectively. The RPBE optimized lattice constants for the metal crystals were used (Cu: 3.71, Au: 4.22, Ag: 4.21, Pt: 4.02, Ni: 3.56, Ir: 3.87, Rh: 3.85, and Fe: 2.91), and the slab was separated from its periodic images by at least 12 Å of vacuum. The dipole correction was used in all cases to remove electrostatic interaction between the periodic images of the slab. The atomic structure of the various reactants and products was found by minimizing the energy until the magnitude of atomic forces had dropped below 0.03 eV/Å.

In some of the calculations presented here, the TCM model was used (Figure 2 and Figures S3 and S5−S6). There the change in free energy of the system at each elementary step was estimated by first calculating the free energy without applied potential. This involves calculating the energy of the system, zero-point energy (ZPE) and vibrational entropy of adsorbed species using the harmonic approximation and using table values for the ZPE and entropy for gas-phase species.[69,70] The free energy was then adjusted for the presence of the applied potential by adding a free energy contribution of $-neU$ for each electron that reacts, where $-e$ is the charge of the electron and U is the applied potential.[27] In the TCM, this procedure is used to estimate the onset potential of a reaction, assuming the rate becomes appreciable when no elementary step is uphill in free energy.[30,32,36] However, in the calculations presented here, the activation energy of each elementary step was evaluated

DOI: 10.1021/acscatal.7b03308
ACS Catal. 2018, 8, 5240−5249

from CI-NEB calculations and the applied potential estimated explicitly using the methods described above.

RESULTS AND DISCUSSION

Mechanism of CO_2RR to Hydrocarbons and Alcohols on Cu(111). The first elementary step of CO_2RR is the addition of a proton to CO_2 and extraction of an electron from the electrode to form *COOH (an asterisk, *, indicates adsorption to the surface). For the relevant range in applied potential, around −1.0 V, this step has low activation energy (0.2−0.35 eV) for all the metal electrodes studied, except Au and Ag where the value is between 0.6 and 1.0 eV. On Au and Ag it turns out to be the rate-limiting step (Figure S7). Several of the following steps on Cu(111) are slower. The simulated system and the atomic scale mechanism of two of the slowest steps in CO_2RR on the Cu(111) surface are illustrated in Figure 1 (other steps are shown in Figure S8). The MEPs for several proton−electron transfer reactions are shown. A solvated proton gets transferred by a Grotthuss-type mechanism toward the electrode and attaches to the admolecule at the same time that an electron is brought in from the electrode. The assumption here is that the coupling is strong enough for the process to be adiabatic so the MEP on the ground state electronic surface gives the reaction path with highest statistical weight. As can be seen from Figure 1, the process involves large relaxation of the reactant molecule as well as the neighboring H_2O molecules and even some of the H-adatoms on the surface. Some of the Cu surface atoms move by more than 0.3 Å along the path.

One of the critical steps is the reduction of CO. The activation energy for the formation of *CHO turns out to be significantly higher than for *COH formation, as can be seen from Figure 1. The reason is that the path the solvated proton takes to reach the O atom is shorter than the path to reach the C atom of *CO and also the fact that the electronegativity of the O atom is greater than that of the C atom. Without applied potential, *CHO can form with a lower activation energy by a surface hydrogenation reaction, where an H-adatom attaches to the *CO, but the proton−electron transfer reaction to form *COH is favored when a potential of $U < -0.6$ V is applied (Figure S9).

The reduction of *COH could lead to the formation of a C-adatom and a water molecule, as has previously been proposed,[39] but the activation energy is significantly lower for *CHOH formation by a proton−electron transfer step, only 0.07 eV (see Figure 1 and Figure 2).

The calculated free energy diagram for CO_2RR to form CO, CH_4, C_2H_4, CH_3OH, and C_2H_5OH on Cu(111) in the presence of −0.9 V potential is shown in Figure 2 along with the calculated activation energy for each step (see also Figure S10). The highest activation energy for methane formation is 0.45 eV for the reduction of *CO to *COH. This reaction mechanism for CH_4 formation by CO_2RR had been presented earlier,[43,44] as was mentioned in the Introduction. Here, the mechanism for several other products is presented. The activation energy for CH_3OH formation by reduction of $*CH_2OH$ is 0.39 eV and involves a surface hydrogenation reaction step. There, a proton is first transferred to the surface where it combines with an electron via a Volmer reaction and then $*CH_2OH$ is hydrogenated to methanol. As discussed below, the Volmer reaction has an even higher activation energy of 0.75 eV at −0.9 V, and becomes the rate-limiting step for methanol formation. The alternative step at this stage is the

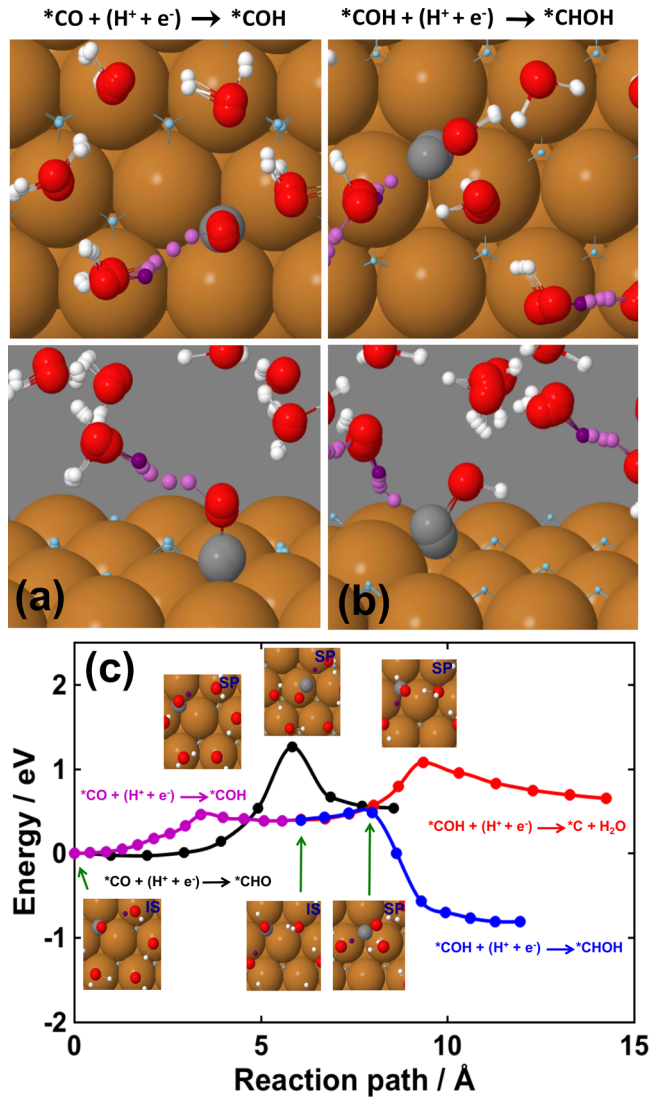

Figure 1. Minimum energy paths for two steps in the optimal CO_2RR mechanism at a Cu(111) electrode. (a) and (b): Five positions of the transferred proton (purple, with a darker color representing the initial state), the H atoms (blue for adatoms, white in H_2O molecules), O atoms (red), and C atoms (gray) starting with the initial state and ending at the saddle point on the energy surface. Only the initial configuration of the Cu atoms is shown for clarity. (c) Energy along the minimum energy paths for elementary proton−electron transfer steps where the initial state corresponds to −0.9 V potential. First, reduction of *CO to *COH (purple curve) and to *CHO (black curve). Second, *COH is further reduced to form *CHOH (blue curve) or *C and H_2O (red curve). The calculations shown here are for a finite system where the applied potential changes along the path. The activation energy obtained from an extrapolation to an infinite system is given in Figure 2.

formation of $*CH_2$ and H_2O, which has an activation energy of only 0.21 eV at −0.9 V. As discussed above, the rate-limiting step for methane formation has an activation energy of 0.45 eV at −0.9 V. As a result, methane is mainly formed rather than methanol in CO_2RR, unlike the industrial process where CO_2 reacts with H_2 gas. The O atom that sticks out from the surface is more accessible to the solvated proton coming in from the water phase than the C atom which is bound to the surface.

The presence of $*CH_2$ as an intermediate explains how C−C bond formation can occur on the Cu(111) surface. Two $*CH_2$

DOI: 10.1021/acscatal.7b03308
ACS Catal. 2018, 8, 5240−5249

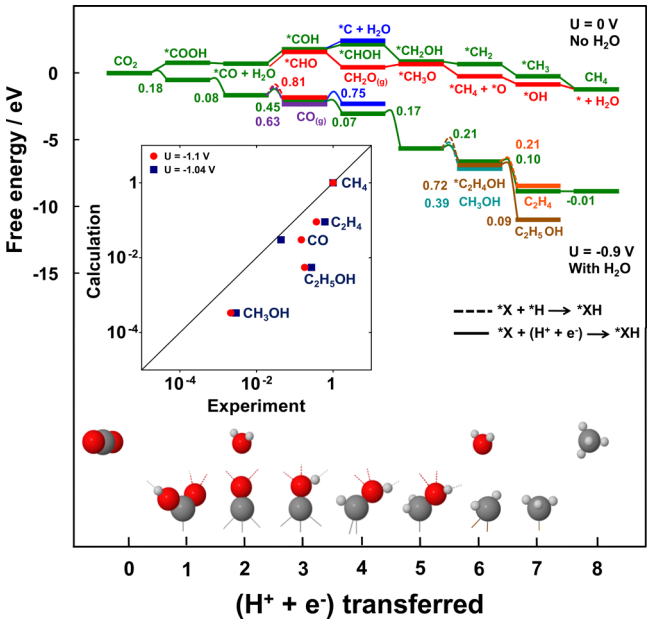

Figure 2. Calculated free energy and activation energy in CO_2RR at a Cu(111) electrode and comparison of predicted current density with experiment. Lower green curve: the optimal mechanism for methane formation when a potential of −0.9 V is applied and water is present. Upper green curve: neither applied potential nor water present. Purple curve: CO desorbs from the surface. Red curves: *CHO is formed rather than *COH. Blue curves: *C is formed rather than *CHOH. Cyan curve: methanol is formed. Brown curve: ethanol is formed. Orange curve: ethylene is formed. The numbers give the activation energy in eV. The inset graph shows a comparison of the calculated and experimentally measured[16] current density at two applied potentials and Cu(111) electrode for the five main products, normalized to the current density for methane formation. The agreement is excellent, considering that no parameter is adjusted in the calculations except that we assume a typical value of the pre-exponential factors, the same for all the elementary steps. The inset at the bottom show the optimal structure of the admolecules and bonds they form to the surface (solid lines) and hydrogen bonds to nearby H_2O molecules (dashed lines) as well as the reactant CO_2, and CH_4 and H_2O product molecules.

admolecules can combine to form C_2H_4 with an activation energy that is only 0.11 eV higher than the reduction of $*CH_2$ to $*CH_3$ (Figure 2 and Figure S10). As a result, the rate of methane formation is predicted to be only slightly higher than ethylene formation. The intermediates $*CH_2OH$ and $*CH_2$ can also combine to make a C−C bond to form $*C_2H_4OH$ which then gets hydrogenated to C_2H_5OH. The reaction path presented here for C−C bond formation on the Cu(111) surface is different from previously proposed mechanisms based on CO−CO, CO−CHO, or CO−COH species.[41,49,51] It is known, however, from experiments that the overpotential for ethylene formation on the Cu(100) surface is lower than for HCA formation on the Cu(111) surface.[7] The mechanism of ethylene formation appears to be entirely different for the Cu(100) and Cu(111) surfaces.

Comparison with Experiments. The relative abundance of products deduced from the calculations described above is in good agreement with experimental measurements. First of all, the fact that formaldehyde (CH_2O) is not predicted to be an intermediate (unlike a previously proposed mechanism[30−32]) agrees with experimental observations of Schouten et al.[6] A quantitative comparison between the calculated activation energy and experimental measurements of current density associated with each of the products can be made by assuming a typical pre-exponential factor in the Arrhenius rate expression and using the rate-limiting step approximation (see Methods section). The difference in activation energy of methanol vs methane formation at −1.1 V, 0.60−0.40 eV, then predicts ≃3 orders of magnitude difference in the current density associated with these two products at room temperature, in close agreement with measurements on Cu(111), where a difference of 2.5 orders of magnitude was obtained.[8,14] The calculated current density for the various products is shown in the inset of Figure 2, where we normalize the current density with respect to methane. The agreement with the experimental measurements is excellent, considering that the calculations contain no adjustable parameters except that we assume a typical value of the pre-exponential factor, the same for all the elementary steps. Since the calculations can only be done at discrete values of the applied potential, an interpolation is made between −0.9 and −1.3 V to obtain the values reported from the experimental measurements, −1.04 and −1.1 V.

The activation energy of proton−electron transfer reaction steps is strongly dependent on the strength of the applied potential. One example is the protonation of *CO to *COH, shown in Figure S9. The rate-limiting step (i.e., the step for which the highest saddle point is reached with respect to the reactants or the lowest energy of a preceding intermediate), also changes as the applied potential is varied, as shown in Figure 3a. For Cu(111), a crossover occurs at −0.6 V as the activation energy for CO_2 reduction to methane becomes lower than for hydrogen evolution. The applied potential at this calculated crossover corresponds well to the potential at which methane starts to form at a significant yield in the experiments.[3,6,8,14] The current density associated with CH_4 formation is predicted to increase by 7 orders of magnitude as the applied potential is varied from −0.3 to −0.9 V. The variation of the activation energy, current density, and current efficiency with applied voltage is shown in Figure 3, and comparison made with experimental results on both Cu(111)[13,16] and polycrystalline Cu.[8] Again, the calculations reproduce well the various experimental measurements. This good agreement lends strong support for our simulation methodology, the model used here for the electrode/electrolyte, and the reaction mechanism we have identified. Similar close agreement between calculations and measurements has been obtained for the other metals (see Figure 3 and Figures S11, S12).

Hydrogen Evolution Reaction on Cu(111). A key issue for the CO_2RR to hydrocarbons and alcohols is the rate of the competing reaction, HER, where a proton does not attach to the carbon containing admolecule but rather adsorbs on the surface (the Volmer reaction) and then forms an H_2 molecule either by reacting with a solvated proton (Heyrovsky reaction), or another adsorbed H-adatom (Tafel reaction). We have calculated the activation energy and the current density of HER by both mechanisms as a function of applied potential (Figure 3 and Figures S11, S12, S13, S14). For the Volmer−Tafel reaction, which is the dominant mechanism in the relevant range of applied potential, the reaction rate is indirectly affected by the applied potential through the potential dependence of the coverage of H-adatoms on the surface.[28] As the applied electric potential is made more negative, H-adatoms occupy more of the 3-fold hollow sites until all such sites have been filled at 1 ML coverage. When the potential is lowered further,

DOI: 10.1021/acscatal.7b03308
ACS Catal. 2018, 8, 5240−5249

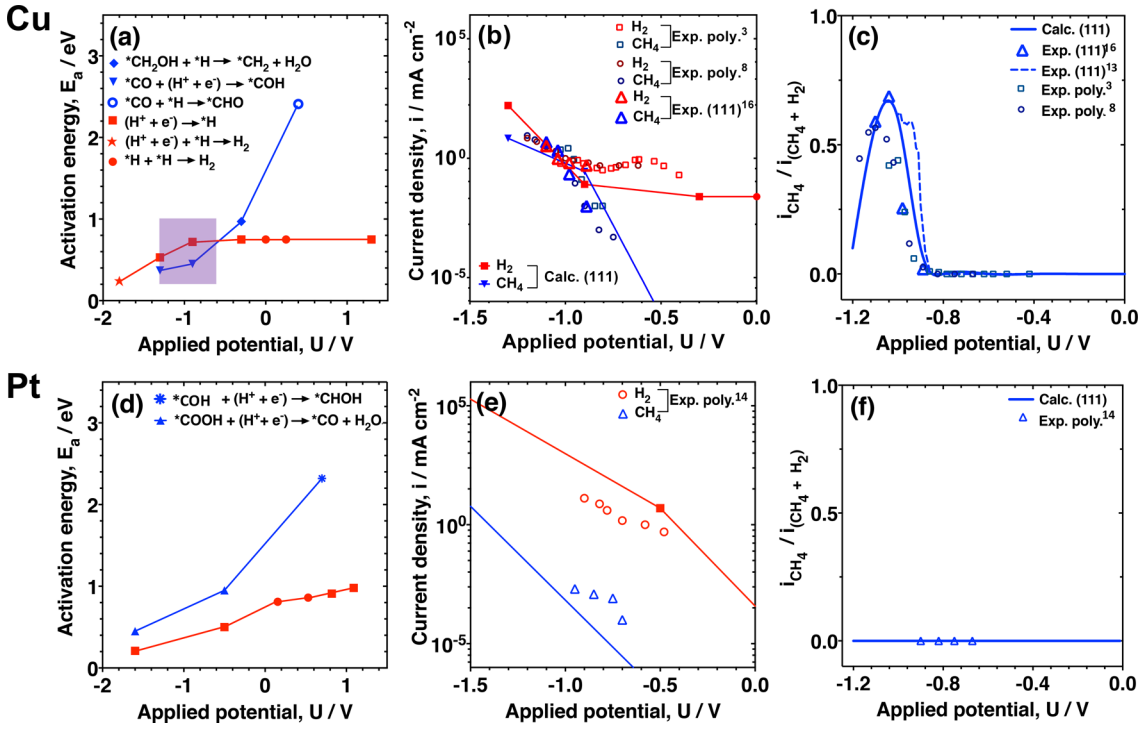

Figure 3. Calculated activation energy of the rate limiting steps in CO_2RR to methane and hydrogen evolution reaction, and comparison of calculated and measured current density and current efficiency. Calculated activation energy at (a) Cu(111) and (d) Pt(111) surfaces as a function of applied potential (some of the data points are taken from ref 44). The purple shaded area highlights the important region where the activation energy for CO_2RR is lower than for HER. Legend in (a) applies also to (d). Calculated and measured[3,8,13,14,16] current density for CH_4 and H_2 formation on (b) Cu and (e) Pt electrodes. The calculations are for Cu(111) and Pt(111) surfaces and the experimental measurements are for Cu(111),[16] polycrystalline Cu,[3,8] and polycrystalline Pt[14] surfaces. Legend in (b) applies also to (e). The symbols are defined in (a) and (d). Current efficiency in CO_2 reduction as a function of applied potential for (c) Cu(111) and (f) Pt(111) electrodes. The current efficiency is calculated by dividing the current density for methane formation with the total current density for methane and hydrogen formation. Experimental results[3,8,13,14,16] (open symbols and dashed line) and theoretical calculations (solid lines). $CH_{4(g)}$ forms at the Cu electrode in a narrow potential window between −0.9 and −1.2 V, but $H_{2(g)}$ is formed at the Pt electrodes for all values of the applied potential.

H-adatoms start to occupy on-top sites where the binding is weaker than at 3-fold hollow sites[28] (Figure S3). The activation energy for associative desorption of H_2 depends strongly on which sites the H-adatoms occupy (Figure S14d). As long as the on-top sites are not populated, the activation energy for H_2 formation is high. However, when H-adatoms are present at on-top sites, the HER by Tafel reaction becomes fast. A special feature of the Cu(111) surface is the low differential adsorption energy of H atoms at on-top sites. An applied potential of −1.3 V is required in order to populate the on-top sites (Figure S3). As a result, CO_2RR has lower activation energy than HER on Cu(111) over a range of applied potential from −0.6 to −1.6 V, see Figure 3a. When the applied potential becomes more negative than −1.6 V, the electrode is predicted to be fully covered with H-adatoms and no carbon containing species present (Figure S3). The Volmer reaction then becomes the rate-limiting step (Figures S11, S14b, and S15).

Comparison with Other Metals. Calculated results for Pt(111) electrodes are shown in Figure 3. From the TCM, one could conclude that Pt(111) is an even better CO_2RR catalyst than Cu(111) because the onset potential is predicted to be only −0.35 V as compared with −0.85 V on Cu(111) (Figures S5 and S6). The onset potential predicted for the stepped Pt(211) and Cu(211) surfaces are, however, more similar (see Figure S6c and ref 32) and in reasonable agreement with experiments.[14] The activation energy for CO_2RR is larger than for HER on Pt(111), for the whole range in applied potential as shown in Figure 3d. The calculated current density for HER is in close agreement with experimental measurements and is orders of magnitude larger than for CO_2RR, see Figure 3e,f. This is in stark contrast to the trends observed on the Cu(111) electrode, where the rate of CO_2RR becomes higher than the rate of HER at around −0.85 V (Figure 3b).

Similar calculations were carried out for Au(111), Ag(111), Ni(111), Fe(110), Ir(111), and Rh(111) surfaces (Figure 4 and Figures S3, S5, S6, S7, S11, S12, S13, S14, and S15). The reaction paths for methane and CO formation are found to be more or less the same for all the metals studied at around −1.0 V, whereas the rate-limiting steps may differ. However, the reaction paths are highly sensitive to the applied potential. Below, the calculated rate and current efficiency for various metals is presented as a function of applied potential. Calculated current efficiency corresponding to CO_2 reduction to methane or CO formation at the various metals is shown as a function of applied potential and compared with the experimental results of Kuhl et al.[14] in Figure 4 (see also Figures S11 and S13). The current efficiency is now shown as a function of both CO adsorption energy and applied potential. No significant current efficiency is predicted for CO_2RR on Pt(111), Ni(111) and Fe(110) in agreement with the experimental results. Nearly all of the current goes into formation of H_2 gas. The calculations indicate that Cu(111) actually has similar activity for CO_2RR as Rh(111), Ni(111), and Ir(111) over the potential range from 0 to −1.2 V (Figures

DOI: 10.1021/acscatal.7b03308
ACS Catal. 2018, 8, 5240−5249

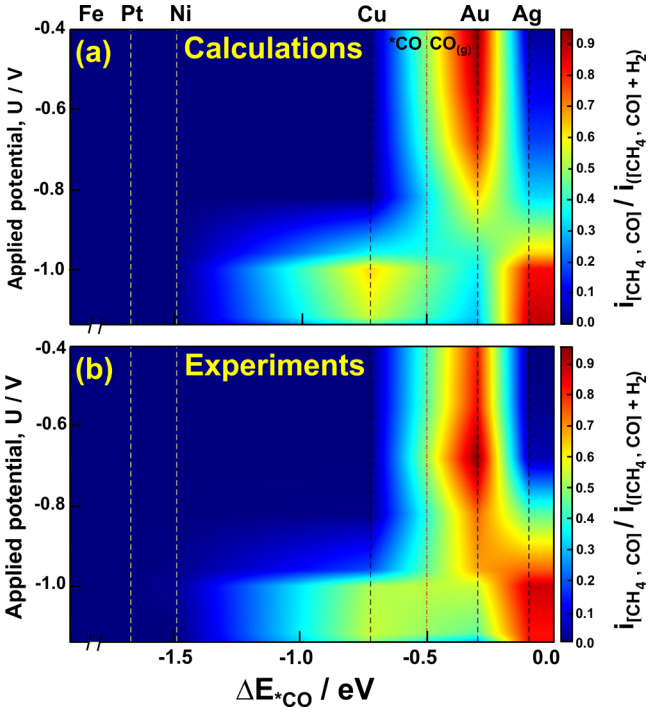

Figure 4. Contour graph showing (a) calculated and (b) measured[14] current efficiency of CO_2 reduction to either CH_4 or CO as a function of applied potential. The red dashed line indicates the binding energy of CO at which adsorbed *CO is in equilibrium with $CO_{(g)}$ (at a partial pressure of 0.01 atm). CO is predicted to desorb when the binding energy is smaller.[32] For Cu, Ni, Pt, and Fe, the current efficiency for CH_4 formation is shown, while $CO_{(g)}$ formation is shown for Au and Ag. The current density for CO_2 reduction and H_2 formation is calculated from the activation energy of the rate-limiting steps for each of the metals as a function of applied potential (Figures S13a,b). The metals are arranged according to the calculated binding energy of CO on the close packed surfaces and a linear interpolation applied between the data points. Significant current associated with CO_2 reduction is obtained for Cu, Ag, and Au (yellow and red regions), while mainly H_2 forms at other metals (blue region).

S13a and S14a) but is a better CO_2RR catalyst because HER is slower (Figures S13b and S14b). A high current efficiency for CO_2RR to CO is calculated for Au(111) at small applied potential but when larger negative potential is applied, the efficiency drops as more H_2 is evolved (Figure 4 and Figure S11). Ag(111) on the other hand evolves H_2 even when the applied potential is small, but CO starts to form at around −0.6 V. The results of the calculations are in close correspondence with the trends observed in the experiments, as shown in Figure 4 and Figures S11 and S12, both with respect to the metal electrode and the applied potential. The overall trend is quite clear with significant CO_2RR current for methane formation on Cu but CO formation on Ag and Au. The CO_2RR current is insignificant for the metals that bind CO more strongly because H_2 formation dominates there. The difference in current density of CO_2RR and of HER is shown in a contour graph in Figure S13c as a function of both applied potential and CO adsorption energy.

The calculated and measured current efficiency at an applied potential for which the CO_2RR current efficiency for methane formation (for Fe, Pt, Ni, and Cu) or CO formation (for Au and Ag) was experimentally found to be maximal is shown in Figure S12. The metals are arranged according to CO binding energy on the close packed surfaces and a linear interpolation applied between the data points. The agreement between the calculated results and the experimentally measured data[14] is remarkably good.

An important result of these calculations is the similarity of the rate of CO_2RR on all the metals studied while the rate of HER is quite different (see Figure S14a,b). The reason is that CO_2RR reactions involve direct proton−electron transfer to the carbon-containing admolecule on the metal surface and hence the metal surface does not play a vital, catalytic role. In HER, however, the protons are first added to the surface (Volmer reaction), and once the applied potential is such that on-top sites become populated (Figure S3), the H_2 is produced rapidly in a Tafel reaction. The metal surface, therefore, plays an important role in determining the rate of HER. The Heyrovsky reaction becomes the preferred mechanism of HER only at even larger negative potentials. Cu, Au and Ag have a small differential H-adsorption energy at on-top sites so a large negative potential is needed to populate those sites[28] (Figure S3). As a result, the rate of HER remains relatively low on Cu, Au and Ag electrodes even when large enough negative potential is applied to make the CO_2RR rate significant. This is the key reason why CO_2 can be reduced to methane on Cu(111) and to CO on Au(111) and Ag(111) while the other metal surfaces mainly give H_2. An important indicator of a good CO_2RR catalyst is, therefore, small H-adsorption energy at on-top sites.

Descriptors for High Yields of Hydrocarbons and Alcohols. Since full electrochemical simulations—as the ones described above where the solid/liquid interface is modeled and activation energy evaluated as a function of applied voltage—are computationally demanding, it is important to develop a simple descriptor that can help identify the more promising catalyst materials. Previously, the CO binding energy has been used as a descriptor,[32] and more recently both CO and H binding energy have been used as a two-parameter descriptor.[71] There, the H binding energy descriptor was computed for a low H coverage. Our results show, however, that in order to describe well enough the rate of the competing reaction, HER, it is necessary to use the differential adsorption energy of H-adatoms at on-top sites while all the 3-fold hollow FCC sites are occupied by H atoms (beyond 1 ML H coverage). Only when the binding energy of H-adatoms at on-top sites is weak enough can the large negative potential needed for CO_2RR be applied without HER becoming the dominant reaction (Figures S3 and S16a,b). For some of the metals considered here, the calculated differential hydrogen binding energy indicates that H atoms can occupy some of the subsurface sites before on-top sites become occupied, see Table S2. This has only a minor effect on the binding energy of H atoms at on-top sites, the key descriptor proposed here, and does not change the trends and conclusions obtained here. Figure 5 shows the ratio of CO_2RR and HER for 24 metal electrodes as a function of two descriptors: The CO binding energy and the differential adsorption energy of H-adatoms at on-top sites. The combination of these two descriptors predicts the ratio correctly for the 24 metal electrodes that have been tested experimentally. Most metals, including Pt, are located in the region where H-adatom binding at on-top sites is strong and as a result H_2 gas is mainly formed (blue region). For metals with weaker H-adatom binding at on-top sites, the H_2 formation is smaller. Cu lands in the region where formation of hydrocarbons and alcohols is of the same order as the formation of

DOI: 10.1021/acscatal.7b03308
ACS Catal. 2018, 8, 5240−5249

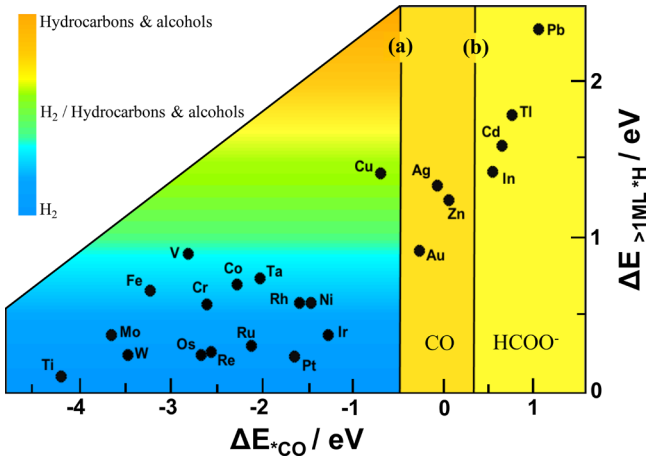

Figure 5. Two-parameter descriptor of the electrocatalytic activity of metal electrodes. Relative rate of CO_2 reduction and H_2 formation is shown as a function of the binding energy of an isolated CO molecule (horizontal axis) and differential adsorption energy of an H-adatom at an on-top site (vertical axis), occupied once the coverage exceeds one monolayer. Cu is unique in that the latter is small while the adsorption energy of CO is large enough for it to undergo reduction all the way to hydrocarbons and alcohols. Smaller CO adsorption energy, designated by line (a), results in desorption of CO or, to the right of line (b), release of $HCOO^-_{(aq)}$. Large differential adsorption energy of H-adatoms at on-top sites leads to H_2 formation (blue area) rather than CO_2RR.

H_2 (green). None of the pure metals are located in the region where formation of hydrocarbons and alcohols dominates over H_2 formation (dark yellow). For metals where the CO binding is weak, the reduction stops at CO because the molecules desorb, as is observed for Ag, Zn and Au electrodes.[5,14] For even weaker CO binding, the reduction stops at $HCOO^-$, as has been observed for Tl, Pb, In and Cd.[5]

The two-parameter descriptor summarizes well the experimental observations and can serve as a first indicator of a good CO_2RR catalyst. In order for CO_2 to be reduced to hydrocarbons or alcohols, the CO binding energy needs to be strong enough for the molecule to stay on the surface and the differential binding energy of *H at on-top sites needs to be small enough for the side reaction, H_2 formation, not to dominate. The two parameters are somewhat correlated, as can be seen from Figure 5, but the scatter is large, which means that it should be possible to find a catalyst with higher CO_2RR catalytic efficiency than Cu. The goal is to find a catalyst that leads to hydrocarbon or alcohol formation at a lower overpotential and less H_2 formation.

CONCLUSIONS

The calculations of CO_2RR and HER presented here for various close-packed electrode surfaces, such as Cu, Pt, Au, Ag, Ni, Rh, Ir, and Fe, using a realistic model of the electrochemical interface and including the effect of applied potential on the activation energy of the various elementary steps, show why Cu is the only metal studied so far for which the reduction goes beyond CO to form hydrocarbons and alcohols. The reason is a crossover in activation energy at around −0.6 V where for CO_2RR becomes more facile than HER, until ca. −1.4 V where the activation energy of HER again becomes lower as the mechanism for HER switches from Volmer−Tafel to Volmer−Heyrovsky. The activation energy for HER remains high for large negative potential because the on-top sites on the Cu(111) surface cannot easily be occupied by H adatoms.

A variation in applied potential also results in shifts in the reaction mechanism of other steps. For example, when the applied potential is around −0.6 V, there is a crossover in the hydrogenation of *CO. For a potential of $U > -0.6$ V, the *CO to *CHO step has lower activation energy, while for $U < -0.6$ V the *CO to *COH has lower activation energy.

It is essential to include the effect of the applied potential on the activation energy of the various elementary steps. As has been pointed out before,[43,44] the optimal mechanism for CH_4 formation at −0.9 V on Cu(111) is entirely different from what the TCM model predicts for all intermediates after *CO; namely *COH, *CHOH, $*CH_2OH$, $*CH_2$, $*CH_3$ and CH_4 as compared to *CHO, $CH_2O_{(g)}$, $*OCH_3$, $CH_{4(g)}$ + *O, *OH, and H_2O obtained with the TCM model. The direct proton−electron transfer reaction turns out to have a lower activation energy than the surface hydrogenation reaction for the reduction of all CO_2RR intermediates in CH_4 formation.

The mechanism and rate of formation of other carbon-containing species on Cu(111) are also presented here. Methanol is formed by surface hydrogenation of $*CH_2OH$. Ethylene is formed when two $*CH_2$ intermediates combine and desorb as C_2H_4. Ethanol is formed when $*CH_2OH$ and $*CH_2$ intermediates combine and form $*C_2H_4OH$ followed by a reduction to ethanol via a direct proton−electron transfer step. The calculated current density corresponding to these products as well as hydrogen formation is found to agree well with the various experimental measurements that have been reported. Cu is unique among these metals in that CO binds strongly enough (while CO desorbs from Ag and Au electrodes), and the binding energy of H-adatoms at on-top sites is low enough for H_2 formation to be relatively slow (while Pt, Ni, Fe, Ir, and Rh mainly form H_2 gas). The calculated current density and current efficiency as a function of applied voltage for the various products and for various metal catalysts is in close agreement with experimental measurements, demonstrating the accuracy of the theoretical approach used here.

A two-parameter descriptor consisting of the differential adsorption energy of H-adatoms at on-top sites and the CO adsorption energy is proposed as a prescreening tool for the identification of the most promising candidates for an improved CO_2RR catalyst. It can predict whether the electroreduction product will be hydrocarbons/alcohols, H_2, CO, or $HCOO^-$. However, in order to predict the selectivity toward a given product, calculations of the activation energy in the various elementary steps need to be carried out to evaluate the reaction rates as a function of applied potential. The results presented here demonstrate that this is indeed possible with the theoretical approach described here.

ASSOCIATED CONTENT

Supporting Information

The Supporting Information is available free of charge on the ACS Publications website at DOI: 10.1021/acscatal.7b03308.

Supporting figures and tables related to the way the applied potential is evaluated, extrapolated energetics, convergence tests, free energy diagrams, and minimum energy paths; all data generated and analyzed in this article for both CO_2RR and HER (PDF)

DOI: 10.1021/acscatal.7b03308
ACS Catal. 2018, 8, 5240−5249

AUTHOR INFORMATION

Corresponding Author

*E-mail: egillsk@hi.is.

ORCID

Javed Hussain: 0000-0003-4127-7447

Hannes Jónsson: 0000-0001-8285-5421

Egill Skúlason: 0000-0002-0724-680X

Notes

The authors declare no competing financial interest.

ACKNOWLEDGMENTS

We thank Marc Koper, Jens K. Nørskov, Andrew Peterson, Jan Rossmeisl and Anna Garden for helpful discussions. This work was supported by Nordic Energy Research through the "Nordic Initiative for Solar Fuel Development", the Icelandic Research Fund, the University of Iceland Doctoral Scholarship Fund, and the Academy of Finland FiDiPro program (grant 263294).

REFERENCES

(1) Lim, X. How to Make the Most of Carbon Dioxide. *Nature* **2015**, *526*, 628−630.

(2) Whipple, D. T.; Kenis, P. J. Prospects of CO_2 Utilization via Direct Heterogeneous Electrochemical Reduction. *J. Phys. Chem. Lett.* **2010**, *1*, 3451−3458.

(3) Hori, Y.; Murata, A.; Takahashi, R. Formation of Hydrocarbons in the Electrochemical Reduction of Carbon Dioxide at a Copper Electrode in Aqueous Solution. *J. Chem. Soc., Faraday Trans. 1* **1989**, *85*, 2309−2326.

(4) Hori, Y.; Wakebe, H.; Tsukamoto, T.; Koga, O. Electrocatalytic Process of CO Selectivity in Electrochemical Reduction of CO_2 at Metal Electrodes in Aqueous Media. *Electrochim. Acta* **1994**, *39*, 1833−1839.

(5) Hori, Y. In *Modern Aspects of Electrochemistry*; Vayenas, C. G., White, R. E., Gamboa-Aldeco, M. E., Eds.; Springer: New York, 2008; Vol. *42*, pp 89−189.

(6) Schouten, K. J. P.; Kwon, Y.; Van der Ham, C.; Qin, Z.; Koper, M. T. M. A New Mechanism for the Selectivity to C1 and C2 Species in the Electrochemical Reduction of Carbon Dioxide on Copper Electrodes. *Chem. Sci.* **2011**, *2*, 1902−1909.

(7) Schouten, K. J. P.; Qin, Z.; Perez Gallent, E.; Koper, M. T. M. Two Pathways for the Formation of Ethylene in CO Reduction on Single-crystal Copper Electrodes. *J. Am. Chem. Soc.* **2012**, *134*, 9864−9867.

(8) Kuhl, K. P.; Cave, E. R.; Abram, D. N.; Jaramillo, T. F. New Insights into the Electrochemical Reduction of Carbon Dioxide on Metallic Copper Surfaces. *Energy Environ. Sci.* **2012**, *5*, 7050−7059.

(9) Tang, W.; Peterson, A. A.; Varela, A. S.; Jovanov, Z. P.; Bech, L.; Durand, W. J.; Dahl, S.; Nørskov, J. K.; Chorkendorff, I. The Importance of Surface Morphology in Controlling the Selectivity of Polycrystalline Copper for CO_2 Electroreduction. *Phys. Chem. Chem. Phys.* **2012**, *14*, 76−81.

(10) Reske, R.; Duca, M.; Oezaslan, M.; Schouten, K. J. P.; Koper, M. T. M.; Strasser, P. Controlling Catalytic Selectivities During CO_2 Electroreduction on Thin Cu Metal Overlayers. *J. Phys. Chem. Lett.* **2013**, *4*, 2410−2413.

(11) Varela, A. S.; Schlaup, C.; Jovanov, Z. P.; Malacrida, P.; Horch, S.; Stephens, I. E.; Chorkendorff, I. CO_2 Electroreduction on Well-Defined Bimetallic Surfaces: Cu Overlayers on Pt(111) and Pt(211). *J. Phys. Chem. C* **2013**, *117*, 20500−20508.

(12) Kortlever, R.; Tan, K.; Kwon, Y.; Koper, M. T. M. Electrochemical Carbon Dioxide and Bicarbonate Reduction on Copper in Weakly Alkaline Media. *J. Solid State Electrochem.* **2013**, *17*, 1843−1849.

(13) Schouten, K. J. P.; Perez Gallent, E.; Koper, M. T. M. The Influence of pH on the Reduction of CO and CO_2 to Hydrocarbons on Copper Electrodes. *J. Electroanal. Chem.* **2014**, *716*, 53−57.

(14) Kuhl, K. P.; Hatsukade, T.; Cave, E. R.; Abram, D. N.; Kibsgaard, J.; Jaramillo, T. F. Electrocatalytic Conversion of Carbon Dioxide to Methane and Methanol on Transition Metal Surfaces. *J. Am. Chem. Soc.* **2014**, *136*, 14107−14113.

(15) Singh, M. R.; Kwon, Y.; Lum, Y.; Ager, J. W.; Bell, A. T. Hydrolysis of Electrolyte Cations Enhances the Electrochemical Reduction of CO_2 over Ag and Cu. *J. Am. Chem. Soc.* **2016**, *138*, 13006−13012.

(16) Hahn, C.; Hatsukade, T.; Kim, Y.-G.; Vailionis, A.; Baricuatro, J. H.; Higgins, D. C.; Nitopi, S. A.; Soriaga, M. P.; Jaramillo, T. F. Engineering Cu Surfaces for the Electrocatalytic Conversion of CO_2: Controlling Selectivity Toward Oxygenates and Hydrocarbons. *Proc. Natl. Acad. Sci. U. S. A.* **2017**, *114*, 5918−5923.

(17) Greeley, J.; Jaramillo, T. F.; Bonde, J.; Chorkendorff, I. B.; Nørskov, J. K. Computational High-Throughput Screening of Electrocatalytic Materials for Hydrogen Evolution. *Nat. Mater.* **2006**, *5*, 909−913.

(18) Greeley, J.; Stephens, I. E. L.; Bondarenko, A. S.; Johansson, T. P.; Hansen, H. A.; Jaramillo, T. F.; Rossmeisl, J.; Chorkendorff, I.; Nørskov, J. K. Alloys of Platinum and Early Transition Metals as Oxygen Reduction Electrocatalysts. *Nat. Chem.* **2009**, *1*, 552−556.

(19) Nørskov, J. K.; Bligaard, T.; Rossmeisl, J.; Christensen, C. H. Towards the Computational Design of Solid Catalysts. *Nat. Chem.* **2009**, *1*, 37−46.

(20) Nørskov, J. K.; Abild-Pedersen, F.; Studt, F.; Bligaard, T. Density Functional Theory in Surface Chemistry and Catalysis. *Proc. Natl. Acad. Sci. U. S. A.* **2011**, *108*, 937−943.

(21) Gross, A.; Schnur, S. Computational chemistry applied to reactions in electrocatalysis. In *Catalysis in Electrochemistry: From Fundamentals to Strategies for Fuel Cell Development*; Santos, E., Schmickler, W., Eds. John Wiley & Sons, Inc.: Hoboken, NJ, 2011; Chapter 5.

(22) Mueller, J. E.; Fantauzzi, D.; Jacob, T. Multiscale modeling of electrochemical systems. In *Electrocatalysis*; Alkire, R. C., Kolb, D. M., Kibler, L. A., Lipkowski, J., Eds.; Wiley-VCH Verlag GmbH & Co. KGaA: Weinheim, 2013; Vol. *4*.

(23) Nielsen, M.; Björketun, M. E.; Hansen, M. H.; Rossmeisl, J. Towards First Principles Modeling of Electrochemical Electrode-Electrolyte Interfaces. *Surf. Sci.* **2015**, *631*, 2−7.

(24) Zheng, Y.; Jiao, Y.; Jaroniec, M.; Qiao, S. Z. Advancing the Electrochemistry of the Hydrogen-Evolution Reaction Through Combining Experiment and Theory. *Angew. Chem., Int. Ed.* **2015**, *54* (1), 52−65.

(25) Skúlason, E. Modeling Electrochemical Reactions at the Solid-Liquid Interface Using Density Functional Calculations. *Procedia Comp. Sci.* **2015**, *51*, 1887−1896.

(26) Skúlason, E.; Jónsson, H. Atomic Scale Simulations of Heterogeneous Electrocatalysis: Recent Advances. *Advances in Physics X.* **2017**, *2*, 481−495.

(27) Nørskov, J. K.; Rossmeisl, J.; Logadóttir, A.; Lindqvist, L.; Kitchin, J. R.; Bligaard, T.; Jónsson, H. Origin of the Overpotential for Oxygen Reduction at a Fuel-Cell Cathode. *J. Phys. Chem. B* **2004**, *108*, 17886−17892.

(28) Skúlason, E.; Tripkovic, V.; Björketun, M. E.; Gudmundsdóttir, S.; Karlberg, G.; Rossmeisl, J.; Bligaard, T.; Jónsson, H.; Nørskov, J. K. Modeling the Electrochemical Hydrogen Oxidation and Evolution Reactions on the Basis of Density Functional Theory Calculations. *J. Phys. Chem. C* **2010**, *114*, 18182−18197.

(29) Tripković, V.; Skúlason, E.; Siahrostami, S.; Nørskov, J. K.; Rossmeisl, J. The Oxygen Reduction Reaction Mechanism on Pt(111) from Density Functional Theory Calculations. *Electrochim. Acta* **2010**, *55*, 7975−7981.

(30) Peterson, A. A.; Abild-Pedersen, F.; Studt, F.; Rossmeisl, J.; Nørskov, J. K. How Copper Catalyzes the Electroreduction of Carbon Dioxide into Hydrocarbon Fuels. *Energy Environ. Sci.* **2010**, *3*, 1311−1315.

(31) Durand, W. J.; Peterson, A. A.; Studt, F.; Abild-Pedersen, F.; Nørskov, J. K. Structure Effects on the Energetics of the Electro-

DOI: 10.1021/acscatal.7b03308
ACS Catal. 2018, 8, 5240−5249

chemical Reduction of CO_2 by Copper Surfaces. *Surf. Sci.* **2011**, *605*, 1354−1359.
(32) Peterson, A. A.; Nørskov, J. K. Activity Descriptors for CO_2 Electroreduction to Methane on Transition-Metal Catalysts. *J. Phys. Chem. Lett.* **2012**, *3*, 251−258.
(33) Tripkovic, V.; Vanin, M.; Karamad, M.; Björketun, M. E.; Jacobsen, K. W.; Thygesen, K. S.; Rossmeisl, J. Electrochemical CO_2 and CO Reduction on Metal-Functionalized Porphyrin-Like Graphene. *J. Phys. Chem. C* **2013**, *117*, 9187−9195.
(34) Karamad, M.; Tripkovic, V.; Rossmeisl, J. Intermetallic Alloys as CO Electroreduction Catalysts-Role of Isolated Active Sites. *ACS Catal.* **2014**, *4*, 2268−2273.
(35) Lim, H. K.; Shin, H.; Goddard, W. A.; Hwang, Y. J.; Min, B. K.; Kim, H. Embedding Covalency into Metal Catalysts for Efficient Electrochemical Conversion of CO_2. *J. Am. Chem. Soc.* **2014**, *136*, 11355−11361.
(36) Li, Y.; Chan, S. H.; Sun, Q. Heterogeneous Catalytic Conversion of CO_2: A Comprehensive Theoretical Review. *Nanoscale* **2015**, *7*, 8663−8683.
(37) Steinmann, S. N.; Michel, C.; Schwiedernoch, R.; Sautet, P. Impacts of Electrode Potentials and Solvents on the Electroreduction of CO_2: A Comparison of Theoretical Approaches. *Phys. Chem. Chem. Phys.* **2015**, *17*, 13949−13963.
(38) Cheng, M. J.; Clark, E. L.; Pham, H. H.; Bell, A. T.; Head-Gordon, M. Quantum Mechanical Screening of Single-Atom Bimetallic Alloys for the Selective Reduction of CO_2 to C1 Hydrocarbons. *ACS Catal.* **2016**, *6*, 7769−7777.
(39) Nie, X.; Esopi, M. R.; Janik, M. J.; Asthagiri, A. Selectivity of CO_2 Reduction on Copper Electrodes: The Role of the Kinetics of Elementary Steps. *Angew. Chem., Int. Ed.* **2013**, *52*, 2459−2462.
(40) Nie, X.; Luo, W.; Janik, M. J.; Asthagiri, A. Reaction Mechanisms of CO_2 Electrochemical Reduction on Cu(111) Determined with Density Functional Theory. *J. Catal.* **2014**, *312*, 108−122.
(41) Xiao, H.; Cheng, T.; Goddard, W. A.; Sundararaman, R. Mechanistic Explanation of the pH Dependence and Onset Potentials for Hydrocarbon Products from Electrochemical Reduction of CO on Cu (111). *J. Am. Chem. Soc.* **2016**, *138*, 483−486.
(42) Liu, X.; Xiao, J.; Peng, H.; Hong, X.; Chan, K.; Nørskov, J. K. Understanding Trends in Electrochemical Carbon Dioxide Reduction Rates. *Nat. Commun.* **2017**, *8*, 15438−15444.
(43) Hussain, J.; Skúlason, E.; Jónsson, H. Computational Study of Electrochemical CO_2 Reduction at Transition Metal Electrodes. *Procedia Comp. Sci.* **2015**, *51*, 1865−1871.
(44) Hussain, J.; Jónsson, H.; Skúlason, E. Faraday Efficiency and Mechanism of Electrochemical Surface Reactions: CO_2 Reduction and H_2 Formation on Pt(111). *Faraday Discuss.* **2016**, *195*, 619−636.
(45) Calle-Vallejo, F.; Koper, M. T. M. Theoretical Considerations on the Electroreduction of CO to C2 Species on Cu(100) Electrodes. *Angew. Chem., Int. Ed.* **2013**, *52*, 7282−7285.
(46) Montoya, J. H.; Peterson, A. A.; Nørskov, J. K. Insights into C-C Coupling in CO_2 Electroreduction on Copper Electrodes. *ChemCatChem* **2013**, *5*, 737−742.
(47) Luo, W.; Nie, X.; Janik, M. J.; Asthagiri, A. Facet Dependence of CO_2 Reduction Paths on Cu Electrodes. *ACS Catal.* **2016**, *6*, 219−229.
(48) Goodpaster, J. D.; Bell, A. T.; Head-Gordon, M. Identification of Possible Pathways for C-C Bond Formation during Electrochemical Reduction of CO_2: New Theoretical Insights from an Improved Electrochemical Model. *J. Phys. Chem. Lett.* **2016**, *7*, 1471−1477.
(49) Xiao, H.; Cheng, T.; Goddard, W. A. Atomistic Mechanisms Underlying Selectivities in C1 and C2 Products from Electrochemical Reduction of CO on Cu(111). *J. Am. Chem. Soc.* **2017**, *139*, 130−136.
(50) Cheng, T.; Xiao, H.; Goddard, W. A. Full Atomistic Reaction Mechanism with Kinetics for CO Reduction on Cu(100) from ab-initio Molecular Dynamics Free-Energy Calculations at 298 K. *Proc. Natl. Acad. Sci. U. S. A.* **2017**, *114*, 1795−1800.
(51) Garza, A. J.; Bell, A. T.; Head-Gordon, M. Mechanism of CO_2 Reduction at Copper Surfaces: Pathways to C2 Products. *ACS Catal.* **2018**, *8*, 1490−1499.
(52) Varela, A. S.; Ju, W.; Reier, T.; Strasser, P. Tuning the Catalytic Activity and Selectivity of Cu for CO_2 Electroreduction in the Presence of Halides. *ACS Catal.* **2016**, *6*, 2136−2144.
(53) Mills, J. N.; McCrum, I. T.; Janik, M. Alkali Cation Specific Adsorption onto fcc(111) Transition Metal Electrodes. *Phys. Chem. Chem. Phys.* **2014**, *16*, 13699−13707.
(54) Akhade, S. A.; McCrum, I. T.; Janik, M. J. The Impact of Specifically Adsorbed Ions on the Copper-Catalyzed Electroreduction of CO_2. *J. Electrochem. Soc.* **2016**, *163*, F477−F484.
(55) Pérez-Gallent, E.; Marcandalli, G.; Figueiredo, M. C.; Calle-Vallejo, F.; Koper, M. T. Structure and Potential Dependent Cation Effects on CO Reduction at Copper Single-Crystal Electrodes. *J. Am. Chem. Soc.* **2017**, *139*, 16412−16419.
(56) Resasco, J.; Chen, L. D.; Clark, E.; Tsai, C.; Hahn, C.; Jaramillo, T. F.; Chan, K.; Bell, A. T. Promoter Effects of Alkali Metal Cations on the Electrochemical Reduction of Carbon Dioxide. *J. Am. Chem. Soc.* **2017**, *139*, 11277−11287.
(57) Baes, C. F.; Mesmer, R. E. *The Hydrolysis of Cations*; R.E. Krieger Publishing Co.: Malabar, FL, 1986; p 489.
(58) Skúlason, E.; Karlberg, G. S.; Rossmeisl, J.; Bligaard, T.; Greeley, J.; Jónsson, H.; Nørskov, J. K. Density Functional Theory Calculations for the Hydrogen Evolution Reaction in an Electrochemical Double Layer on the Pt(111) Electrode. *Phys. Chem. Chem. Phys.* **2007**, *9*, 3241−3250.
(59) Rossmeisl, J.; Skúlason, E.; Björketun, M. E.; Tripkovic, V.; Nørskov, J. K. Modeling the Electrified Solid-Liquid Interface. *Chem. Phys. Lett.* **2008**, *466*, 68−71.
(60) Filhol, J. S.; Doublet, M. L. An *ab-initio* Study of Surface Electrochemical Disproportionation: The Case of a Water Monolayer Adsorbed on a Pd(111) Surface. *Catal. Today* **2013**, *202*, 87−97.
(61) Schnur, S.; Gross, A. Properties of Metal-Water Interfaces Studied from First Principles. *New J. Phys.* **2009**, *11*, 125003−125029.
(62) Tripkovic, V.; Björketun, M.; Skúlason, E.; Rossmeisl, J. Standard Hydrogen Electrode and Potential of Zero Charge in Density Functional Calculations. *Phys. Rev. B: Condens. Matter Mater. Phys.* **2011**, *84*, 1−11.
(63) Jónsson, H.; Mills, G.; Jacobsen, K. In *Classical and Quantum Dynamics in Condensed Phase Simulations: Proceedings of the International School of Physics*; Berne, B. J., Ciccotti, G., Coker, D. F., Eds.; World Scientific Publishing Co Pte Ltd: Singapore, 1998; p 385.
(64) Henkelman, G.; Uberuaga, B. P.; Jónsson, H. A Climbing Image Nudged Elastic Band Method for Finding Saddle Points and Minimum Energy Paths. *J. Chem. Phys.* **2000**, *113*, 9901−9904.
(65) Henkelman, G.; Jónsson, H. Improved Tangent Estimate in the Nudged Elastic Band Method for Finding Minimum Energy Paths and Saddle Points. *J. Chem. Phys.* **2000**, *113*, 9978−9985.
(66) Hammer, B.; Hansen, L. B.; Nørskov, J. K. Improved Adsorption Energetics within Density-Functional Theory using Revised Perdew-Burke-Ernzerhof Functionals. *Phys. Rev. B: Condens. Matter Mater. Phys.* **1999**, *59*, 7413−7421.
(67) Kresse, G.; Hafner, J. *Ab-initio* Molecular Dynamics for Liquid Metals. *Phys. Rev. B: Condens. Matter Mater. Phys.* **1993**, *47*, 558−0561.
(68) Blöchl, P. E. Projector Augmented-Wave Method. *Phys. Rev. B: Condens. Matter Mater. Phys.* **1994**, *50*, 17953−17979.
(69) Atkins, P. W.; De Paula, J. *Physical Chemistry*; Oxford University Press: Oxford, U.K.2010; p 972.
(70) Hirunsit, P. Electroreduction of Carbon Dioxide to Methane on Copper, Copper-Silver, and Copper-Gold Catalysts: A DFT Study. *J. Phys. Chem. C* **2013**, *117*, 8262−8268.
(71) Bagger, A.; Ju, W.; Varela, A. S.; Strasser, P.; Rossmeisl, J. Electrochemical CO_2 Reduction: A Classification Problem. *ChemPhysChem* **2017**, *18*, 3266−3273.

DOI: 10.1021/acscatal.7b03308
ACS Catal. 2018, 8, 5240−5249